Ultrasonics 52 (2012) 266–275

Contents lists available at SciVerse ScienceDirect

Ultrasonics

journal homepage: www.elsevier.com/locate/ultras

A robust graph-based segmentation method for breast tumors in ultrasound images

Qing-Hua Huang [a,*], Su-Ying Lee [a], Long-Zhong Liu [b], Min-Hua Lu [c], Lian-Wen Jin [a], An-Hua Li [b]

[a] School of Electronic and Information Engineering, South China University of Technology, Guangzhou, China
[b] The Cancer Center of Sun Yat-sen University, Guangzhou, China
[c] Department of Biomedical Engineering, Medical School, Shenzhen University, Shenzhen, China

ARTICLE INFO

Article history:
Received 8 February 2011
Received in revised form 1 August 2011
Accepted 13 August 2011
Available online 25 August 2011

Keywords:
Breast tumor
Graph theory
Image segmentation
Ultrasound

ABSTRACT

Objectives: This paper introduces a new graph-based method for segmenting breast tumors in US images.
Background and motivation: Segmentation for breast tumors in ultrasound (US) images is crucial for computer-aided diagnosis system, but it has always been a difficult task due to the defects inherent in the US images, such as speckles and low contrast.
Methods: The proposed segmentation algorithm constructed a graph using improved neighborhood models. In addition, taking advantages of local statistics, a new pair-wise region comparison predicate that was insensitive to noises was proposed to determine the mergence of any two of adjacent subregions.
Results and conclusion: Experimental results have shown that the proposed method could improve the segmentation accuracy by 1.5–5.6% in comparison with three often used segmentation methods, and should be capable of segmenting breast tumors in US images.

1. Introduction

Breast cancer is one of the leading causes of death in women. Medical ultrasound (US) imaging has been regarded as one of the gold standards for breast tumor imaging, since it is not only inexpensive and fast, but also noninvasive and accurate [1]. However, the manual US image diagnosis is subject to the radiologist's experience and skills. It has been recognized that computer-aided diagnosis (CAD) can increase the efficiency and reduce errors of breast cancer screening by using the computer as a second reader. Segmentation is the most essential and important step for further tumor analysis in CAD system [2].

In the past decade, a large number of segmentation methods including thresholding, neural network (NN), deformable shape model, etc. have been proposed in the literature [3,4]. However, due to the speckles and low contrast which are inherent in the US images, it is often difficult to segment the US images and the detection of boundaries or contours has become an important method to extract the tumor areas. Consequently, the active contour model (ACM) also called Snake [5] has become a popular segmentation method for US images and has been extensively used for breast [6–8], cardiopathy [9,10], carotid artery [11,12], prostate [13,14], thyroid [15,16], etc. For breast tumors in US images, Huang and Chen [6] automatically found the initial contour by the watershed transform for ACM to determine the contours of the tumor. Chang et al. [7] applied an anisotropic filter, a stick procedure and an automatic threshold method to find the initial contours for the Gradient Vector Flow (GVF) Snake, and finally extended this method to 3-D case. Jumaat et al. [8], however, made a comparison between Balloon Snake and GVF Snake in segmenting masses from breast US images and found that the average percentage area difference in the Balloon Snake was much lower than that in the GVF Snake.

The ACM methods deform in an iterative manner to get as close as possible to the contours of breast tumors. They still are sensitive to noises and heavily rely on the initial definition of object contours [6]. Because of the blurry boundaries inherent in the US images, it is difficult to find out an automatic scheme for defining the initial contours. A poorly defined initial contour apparently results in inaccurate segmentation of regions of interest (ROI). Currently used ACM methods require the initial contours to be defined by either manual delineations or some complexly auto -initialized methods. For real-time applications or sequentially processing a large number of images, the contour initialization should be computationally efficient.

In contrast to the ACM methods, clustering, an unsupervised learning technique is an alternative for image segmentation which requires less user participation. Clustering is an iterative method to find clustering centers which minimize the squared distances between sample points and the clustering centers [17]. The image points with varying intensities can be regarded as samples and hence can be grouped into different clusters, which denote non-overlapped regions in the image. Accordingly, the segmentation methods based on clustering techniques are regarded as region

* Corresponding author.
E-mail address: qhhuang@scut.edu.cn (Q.-H. Huang).

0041-624X/$ - see front matter © 2011 Elsevier B.V. All rights reserved.
doi:10.1016/j.ultras.2011.08.011

based methods. *K*-means clustering and fuzzy *C* means (FCM) clustering are the two basic and popular clustering methods [17]. The clustering based segmentation can be automatically performed without the need to set the initial contour. As a result, the *K*-means and FCM have been applied for segmentation of US images [18–20].

Region based segmentation methods based graph theory have also been proposed [21,22]. It is called graph-based (GB) segmentation method. Taking into account global image properties as well as local spatial relationships, a GB method results in a regional map that can be used for further processing, e.g. region merging or labeling. In the GB methods, an undirected graph $G = (V,E)$ where each vertex $v_i \in V$ corresponds to a pixel and an edge $(v_i, v_j) \in E$ connects v_i with v_j is constructed. The edge weights in the graph are often assigned with the difference of intensity, texture or other features between vertices. Consequently, the image segmentation can be converted into the graph segmentation in which each subgraph corresponds to a subregion.

One typical GB segmentation method called efficient graph-based (EGB) algorithm was successfully applied to various images [23]. It consisted of two steps, i.e. the graph construction for mapping an image to a graph, and the mergence of vertices in the graph. Intrinsically, the EGB segmentation method acted as a clustering method and expanded (or merged) regions according to the local spatial, in addition to the global information. Therefore, the regions with similar intensity levels but different locations could be well divided into different segments. Due to their simple structures and reliable theoretical basis, the GB representations and techniques have been refined and extensively applied to many segmentation problems, including medical image segmentations of laparoscopic images [24] and mammograms [25]. To the best of our knowledge, however, little attention has been paid to applying them to US image segmentation due to their significant sensitivity to noises.

Accordingly, we proposed to apply a new GB method to breast tumor segmentation in US images. Due to the complex image artifacts existing in US images, a preprocessing procedure for reducing the speckles and preserving the boundaries was performed before the segmentation. To make the segmentation more robust to noises, a new pair-wise region comparison predicate for our GB method was proposed to segment breast tumor regions. In the new predicate, we took into account the local statistics and the measures of signal-to-noise ratio (SNR) of US images. We designed a new metrics for evaluating the segmentation performance of difference techniques, and conducted experiments to make comparisons among the FCM, *K*-means, EGB and RGB methods. The new GB method was named as robust graph-based (RGB) algorithm because it was relatively insensitive to noises, could be applied with relatively smaller ranges of the parameters, and could improve the segmentation performance in comparison with the EGB method. In addition, we used the FCM and the RGB as the initial contour estimation methods and combined each of them with an ACM (Snake) method together to assess the performance of each algorithm.

The remainder of this paper is organized as follows. The next section describes the new GB method. Then, the experimental results on US images of breast tumor are presented. The final section gives a discussion, draws the conclusions and introduces our future work.

2. Methods

In a GB segmentation method [23], the image was firstly represented by a graph in which each vertex denoted a pixel. An edge existed between each pair of neighboring pixels. The edge weights varied according to some criterion, e.g. intensity difference. The vertices were regarded as the smallest subgraphs at the beginning of the segmentation. A larger subgraph could be generated by merging smaller subgraphs. By repeating the merging procedure, the image could be segmented into several larger homogeneous subregions which were represented by corresponding subgraphs.

In this study, a novel GB method making use of the statistical information of each subgraph (subregion) was proposed. The utilization of the statistics of each subregion could significantly improve the robustness of the proposed method to noises comparing to the EGB method [23]. Hence, it was named as robust graph-based (RGB) segmentation method in this paper.

2.1. Speckle reduction

It is well known that US image often contains plenty of artifacts and noises due to the complex imaging environment and imaging principle, such as speckles and low contrast. They greatly degrade the performance of conventional segmentation methods. To improve the robustness of the RGB method to noises, a preprocessing procedure for speckle reduction was required. A nonlinear anisotropic diffusion (NAD) model which has been proved to be an efficient method for the speckle reduction was used. In this paper, the parameters in the NAD model were set as suggested in [26] (i.e. 10 iterations with a time step $\Delta t = 2$ per iteration, $\alpha^* = 1$, $s = 20$, and $\beta^* = 0.2$).

2.2. Graph construction

In construction of the graph, each vertex $v_i \in V$ corresponded to a pixel in the image, and an edge $(v_i, v_j) \in E$ connected v_i with v_j which were neighbors. For monochrome images, the edge weight w_{ij} was the intensity difference between v_i and v_j, i.e.

$$w_{ij} = |I(v_i) - I(v_j)| \tag{1}$$

where $I(v_i)$ was the intensity of v_i.

In a conventional GB segmentation method, the graph was constructed in an 8-connected neighborhood, i.e. a pixel had eight edges connecting to its neighbors as illustrated in Fig. 1a. One might be wondering whether or not it was necessary to consider all edges connecting any of two neighboring vertices. To answer this question, we took into account three types of graph structure in which a pixel had less edges connecting to its neighbors, i.e. the 6-connected neighborhoods and the 4-connected neighborhoods as illustrated in Fig. 1b–d, respectively. The segmentation performance for the new types of graph was evaluated and an appropriate type of neighborhood was suggested for segmentation of US images. As the number of edges was reduced, the structure of the graph was simplified and the amount of computation was decreased, hence the algorithmic efficiency could be improved.

2.3. Pairwise region comparison predicate

Having constructed a graph in which each subgraph represented a single pixel, we needed to merge these subgraphs with similar intensity levels and form larger subgraphs (i.e. non-overlapped subregions). In this procedure, whether the boundaries

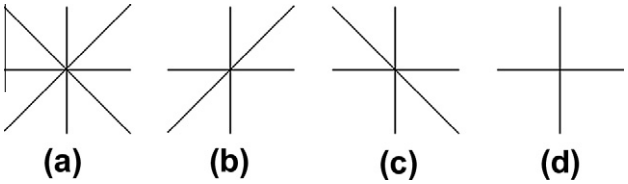

Fig. 1. Four different graph templates where the lines denote the edges, and the intersection point and the endpoints of edges denote the pixels. (a) 8-Connected neighborhood, (b) 6-connected neighborhood (left), (c) 6-connected neighborhood (right), and (d) 4-connected neighborhood.

between two connected smaller subgraphs (subregions) should be eliminated was determined according to a pre-defined predicate that measured the evidence for a boundary between the two subregions.

In the RGB method, we designed a new predicate to determine whether or not two neighboring subregions (i.e. connected subgraphs) should be merged. Given a graph $G = (V,E)$, the resulting predicate $D(C_1,C_2)$ compared the inter-subgraph differences to the within subgraph differences, as expressed by

$$D(C_1,C_2) = \begin{cases} TRUE & \text{if } Dif(C_1,C_2) \leqslant MInt(C_1,C_2) \\ FALSE & \text{otherwise} \end{cases} \quad (2)$$

where $Dif(C_1,C_2)$ was the difference between two subgraphs $C_1, C_2 \subseteq V$, and $MInt(C_1,C_2)$ the minimum internal difference with each subgraph, $C_1, C_2 \subseteq V$. It was reasonable that two subgraphs should be merged if their difference in between was smaller than their minimum internal difference. Consequently, how to define $Dif(C_1,C_2)$ and $MInt(C_1,C_2)$ was the key issue for the segmentation performance.

By taking into account local statistical information, the definition for $Dif(C_1,C_2)$ in the RGB method was expressed as

$$Dif(C_1,C_2) = |\mu(C_1) - \mu(C_2)| \quad (3)$$

where $\mu(C)$ denoted the averaged intensity of subregion C. If there was no edge connecting C_1 and C_2 (i.e. C_1 and C_2 were not spatially adjacent), $Dif(C_1,C_2) = \infty$. It was clear that the mean values for the pixels would be good at reducing the effect of noises.

The definition for $MInt(C_1,C_2)$ was formulated by

$$MInt(C_1,C_2) = \min(Int(C_1) + \tau(C_1), \quad Int(C_2) + \tau(C_2)) \quad (4)$$

where $\tau(C)$, $C \subseteq V$, was a threshold function, and $Int(C)$, $C \subseteq V$, was the internal difference denoted by the standard deviation of C, i.e.

$$Int(C) = \sigma(C) \quad (5)$$

where $\sigma(C)$ was the standard deviation of the pixel intensities in subregion C. The $Int(C)$ represented the extent of deviation of C.

The threshold function τ was defined by

$$\tau(C) = \frac{k}{|C|} \cdot \left(1 + \frac{1}{\alpha \cdot \beta}\right), \quad \beta = \frac{\mu(C)}{\sigma(C)} \quad (6)$$

where α and k took positive values, the $\mu(C)$ and $\sigma(C)$ were the intensity mean and deviation of the subregion C, and $|C|$ was the area of C. We used $\mu(C)/\sigma(C)$ to adjust the influence of $|C|$. $\mu(C)/\sigma(C)$ could be a measure of the smoothness of the subregion C. Note that $\mu(C)/\sigma(C)$ has been usually regarded as a measure of the SNR for a homogeneous region in a US image full of speckles [27]. The lower the $\mu(C)/\sigma(C)$ was, the higher the $\tau(C)$ was. Higher $\tau(C)$ might lead to higher $MInt(C_1,C_2)$, weakening the evidence for the boundary between C_1 and C_2. It is reasonable that two connected inhomogeneous subregions which contain similar textures tend to be merged, resulting in the segmentations being not too fine. On the contrary, higher $\mu(C)/\sigma(C)$ corresponding to a more homogeneous region would strengthen its boundary, decrease the probability of region mergence, and hence make the segmentations not too coarse. The updated threshold function $\tau(C)$ with carefully selected α and k could overcome the problem of over-segmentation to some extent, hence being more robust to noises.

It could be observed that $\tau(C)$ in (6) tended to merge two connected subgraphs when their areas were small. This property would lead to the mergence of smaller subregions and overcome the problem of over-segmentation. It was also worth noting that the selections of α and k in our predicate would significantly influence the segmentation results and their values should be empirically assigned for optimal performance according to the observations of radiologists.

2.4. Region mergence

Based on the proposed pairwise region comparison predicate, any two subregions with similar averaged intensities and a spatial connection could be merged. At the beginning, each vertex in the constructed graph was treated as an isolated subgraph, and each edge was initially treated as being invalid. Then the edges were sorted according to their weights by nondecreasing ordering and traversed. If two vertices connected by an edge being traversed belonged to two different subgraphs and their boundary could be eliminated according to the proposed pair-wise region comparison predicate, the edge was set to be valid and the two subgraphs were merged to form a larger subgraph which was connecting with other subgraphs through invalid edges.

Having traversed all edges, a "forest" including a number of "trees" each of which was a *minimum spanning tree* (MST) could be obtained. A spanning tree of a connected graph G is a tree containing all vertices of G. If the weight of a tree is defined as the sum of the weights of its constituent edges, a MST of G is a spanning tree with the minimum sum of the weights among all spanning trees of G [28]. To obtain a MST, Kruskal [29] proposed to choose the shortest edge which was not yet chosen and did not form any loops with those edges already chosen until no edge could be chosen. If each MST corresponded to a subregion of the image, the pixels locating in the subregion were significantly similar in the feature space whereas those pixels from a different subregion would be significantly different. We used Kruskal's method to obtain MSTs in this study. It was worth noting that the original image was finally divided into a number of homogeneous subregions, each of which could be expressed as a MST.

2.5. The proposed RGB segmentation algorithm

The detailed algorithmic procedures for segmentation of breast tumors in US images were summarized as follows.

1. Performed the speckle reduction and boundary preservation in a US image via the NAD model.
2. Constructed the graph $G = (V,E)$ for the image and set all edges to be invalid.
3. Sorted the edges E into $\pi = (o_1,\ldots,o_m)$ by nondecreasing edge weight. Let $q = 1$.
4. Picked the q-th edge in the sorted edges. If the q-th edge connected different subgraphs and the boundary between the two subgraphs should be eliminated according to the proposed pairwise region comparison predicate shown in (2)–(6), the two subgraphs were merged into a larger subgraph and their edge was set to be valid. The μ and σ of the new subgraph were updated.
5. Let $q = q + 1$. Repeated step 4 until all edges had been traversed.

When all edges had been traversed, each tree in the obtained forest was a MST corresponding to a segmented subregion in the image. Fig. 2 shows the flow chart of the proposed method.

2.6. Experimental methods

This work was approved by Human Subject Ethics Committee of South China University of Technology. Our method was developed using VC++ and evaluated using 20 US images of breast tumors, in which half were benign and the remaining half were malignant. The US images with the subjects' consent forms were provided by the Cancer Center of Sun Yat-sen University and taken from a

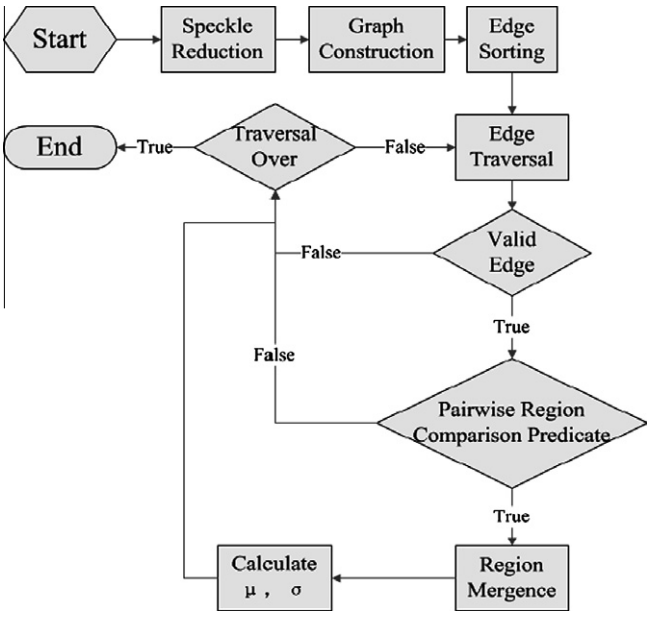

Fig. 2. Flow chart for the robust graph-based segmentation algorithm.

HDI 5000 SonoCT System (Philips Medical Systems) with a L12-5 50 mm Broadband Linear Array at the imaging frequency of 7.1 MHz. The image size was 400 × 300. The "true" tumor regions of the US images were manually defined by three radiologists and averaged.

In order to evaluate the performance of the RGB, three experiments were performed as follows.

1. The graphs were constructed using the four different types of neighborhood as illustrated in Fig. 1, and the segmentation results were compared using five benign and five malignant images so as to find an appropriate type of neighborhood in terms of both segmentation accuracy and computational efficiency.
2. In order to validate the segmentation performance of the RGB, the images were also segmented using the *K*-means [17], FCM [17] and the EGB methods [23], respectively, which have been recognized as efficient region based methods for image segmentation. For the *K*-means and FCM methods, both *K* and *c* (i.e. the numbers of classes), were carefully set to make the target regions isolated from the backgrounds. For the EGB method, the parameter *k* was set to be 150 as suggested in [23] and the "optimal" values which were manually attempted and could mostly isolate the tumor regions without significant over-segmentations according to the judgments of the three radiologists, respectively. In our method, the parameters *k* and α were empirically set to 2000 and 0.01–0.05, respectively.
3. To further verify the performance of the RGB, the contours extracted from FCM and RGB results were treated as the initial contours for Snake, because the region based methods have often been used to initialize a local segmentation for active contours [22]. It is noted that the approximation of initial contours would significantly reduce the iteration runs and computational time of Snake [5]. Therefore, comparing the iteration time and segmentation accuracy of the two contour initialization methods could be another way to verify the performance of the region based segmentation methods. Given the discrete points along the contour, $V = (v_0, v_1, \ldots, v_{n-})$, the Snake algorithm used in this paper minimized a measure of energy as the following formulas [30].

Table 1
The five sets of parameters for the Snake.

No.	*a*	*b*	*c*
1	1.0	2.0	2.0
2	1.0	1.0	1.0
3	2.0	1.0	1.0
4	1.0	2.0	1.0
5	1.0	1.0	2.0

$$E_{Snake}(V) = \sum_{i=0}^{n-1} E_{int}(v_i) + cE_{ext}(v_i) \tag{7}$$

where $E_{int}(v_i)$ and $E_{ext}(v_i)$ were the internal and external energies, respectively. $E_{int}(v_i)$ was defined by

$$\begin{aligned} &E_{\text{int}}(v_i) = a|v'(i)|^2 + b|v''(i)|^2 \\ &|v'(i)|^2 \approx (\bar{d} - |v_i - v_{i-1}|)^2 \Big/ \max_{v_m, w_{m-1} \in V} (\bar{d} - |v_m - v_{m-1}|)^2 \\ &|v''(i)|^2 \approx |v_{i-1} - 2v_i + v_{i+1}|^2 \Big/ \max_{v_m, v_{m-1}, v_{m+1} \in V} (v_{m-1} - 2v_m + v_{m+1})^2 \end{aligned} \tag{8}$$

where $v'(i)$ and $v''(i)$ denoted the first and second derivatives of v_i, *a*, *b* and *c* were the weights balancing the internal and external energies, *d* was the averaged distance between the contour points and the center of the tumor area. $E_{ext}(v_i)$ was defined by

$$\begin{aligned} &E_{ext}(v_i) = -|\nabla I(v_i)|/(\max - \min) \\ &\max = \max_{v_m \in V} \nabla I(v_m) \\ &\min = \min_{v_m \in V} \nabla I(v_m) \end{aligned} \tag{9}$$

where *I* was the image and $\nabla I(v_i)$ was the gradient of the image which attracted *V* to the true contour of the tumor area. The total energy of the contour *V* should be minimized iteratively until it was not significantly changed. That was, at each iteration, the location of v_i should be replaced to minimize the $E_{Snake}(V)$. In order to eliminate the uncertain factors caused by the Snake, five groups of the parameters for *a*, *b*, and *c*, were tested in this study as presented in Table 1.

To assess quantitatively the segmentation accuracy, a metrics called averaged radial error (ARE) was designed as shown in Fig. 3. The ARE was expressed as

$$ARE(n) = \frac{1}{n} \sum_{i=0}^{n-1} \frac{|Cs(i) - Cr(i)|}{|Cr(i) - Co|} \times 100\% \tag{10}$$

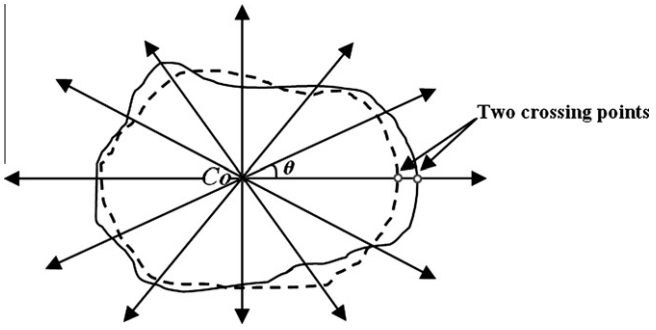

Fig. 3. Illustration of the computation for the averaged radial error. The solid line denotes the "true" boundary of an object and dashed line denotes the boundary produced by a segmentation method. From the center of the region marked by the "true" boundary, a number of rays are emitting and crossing the two boundaries. The percentage of the absolute difference between the two crossing points on each of the rays to the distance from *Co* to the crossing point at the "true" boundary are summed and then averaged as a metric for evaluating the segmentation accuracy.

where n was the number of radial rays emitting from the center (Co) of the "true" tumor region, $Cs(i)$ the location of the pixel at which the boundary of the segmented breast tumor region was crossing the ith ray, and $Cr(i)$ the location of the pixel at which the boundary of the "true" tumor region was crossing the ith ray. The n rays were evenly emitted from Co. In this study, n was set to be 36, i.e. the angle θ between any of two adjacent rays was 10°.

Moreover, the segmentation performance was also evaluated using the method reported by [31]. In that work, three measures including False Negative volume fraction (FNVF), False Positive volume fraction (FPVF), and True Positive volume fraction (TPVF) were defined to evaluate the segmentation accuracy. The FNVF denoted the fraction of tissue defined in the "true" tumor region that was missed by a segmentation method. The FPVF denoted the amount of tissue falsely identified by a segmentation method as a fraction of the total amount of tissue in the "true" tumor region. The TPVF indicated the total fraction of tissue in the "true" tumor region with which the segmented region overlapped. It is obvious that a larger TPVF, smaller FNVF and smaller FPVF would lead to improved segmentation performance.

3. Experimental results

3.1. Qualitative analysis

For brevity, we present the segmentation results for only four typical breast tumors in this paper. Figs. 4a, 5a, 6a and 7a show two benign tumors and two malignant tumors, respectively. After applying the NAD model to the images, the processed images in which most of speckles had been removed can be seen in Figs. 4b, 5b, 6b, and 7b. Based on the preprocessed images, the segmentation results using the K-means are illustrated in Figs. 4c, 5c, 6c and 7c, those using the FCM in Figs. 4d, 5d, 6d, and 7d, those using the EGB ($k = 150$) in Figs. 4e, 5e, 6e and 7e, those using the EGB with the appropriate values of k in Figs. 4f, 5f, 6f and 7f, those using the RGB with the 4-connected neighborhood in Figs. 4g, 5g, 6g and 7g, those using the RGB with the 6-connected neighborhood (right) in Figs. 4h, 5h, 6h and 7h, those using the RGB with the 6-connected neighborhood (left) in Figs. 4i, 5i, 6i and 7i, and those using the RGB with the 8-connected neighborhood in Figs. 4j, 5j, 6j and 7j.

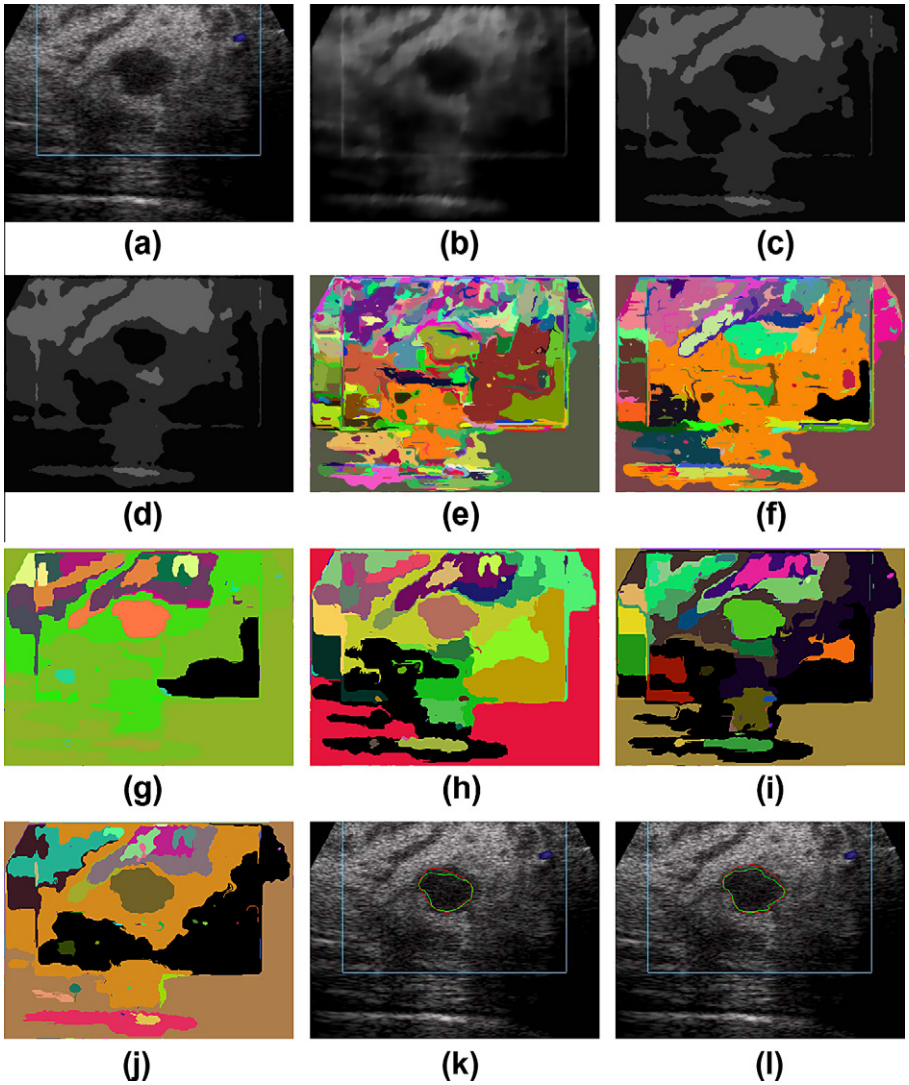

Fig. 4. Segmentation results for the first benign breast tumor. (a) Source image; (b) filtered image; (c) the K-means result, $K = 3$; (d) the FCM result, $C = 3$; (e) the EGB result, $k = 150$; (f) the EGB result, $k = 1200$; (g) the RGB result using the 4-connected neighborhood, $k = 2000$, $\alpha = 0.04$; (h) the RGB result using the 6-connected neighborhood (right), $k = 2000$, $\alpha = 0.04$; (i) the RGB result using the 6-connected neighborhood (left), $k = 2000$, $\alpha = 0.05$; (j) the RGB result using the 8-connected neighborhood, $k = 2000$, $\alpha = 0.02$; (k) the FCM + Snake result; and (l) the RGB + Snake result.

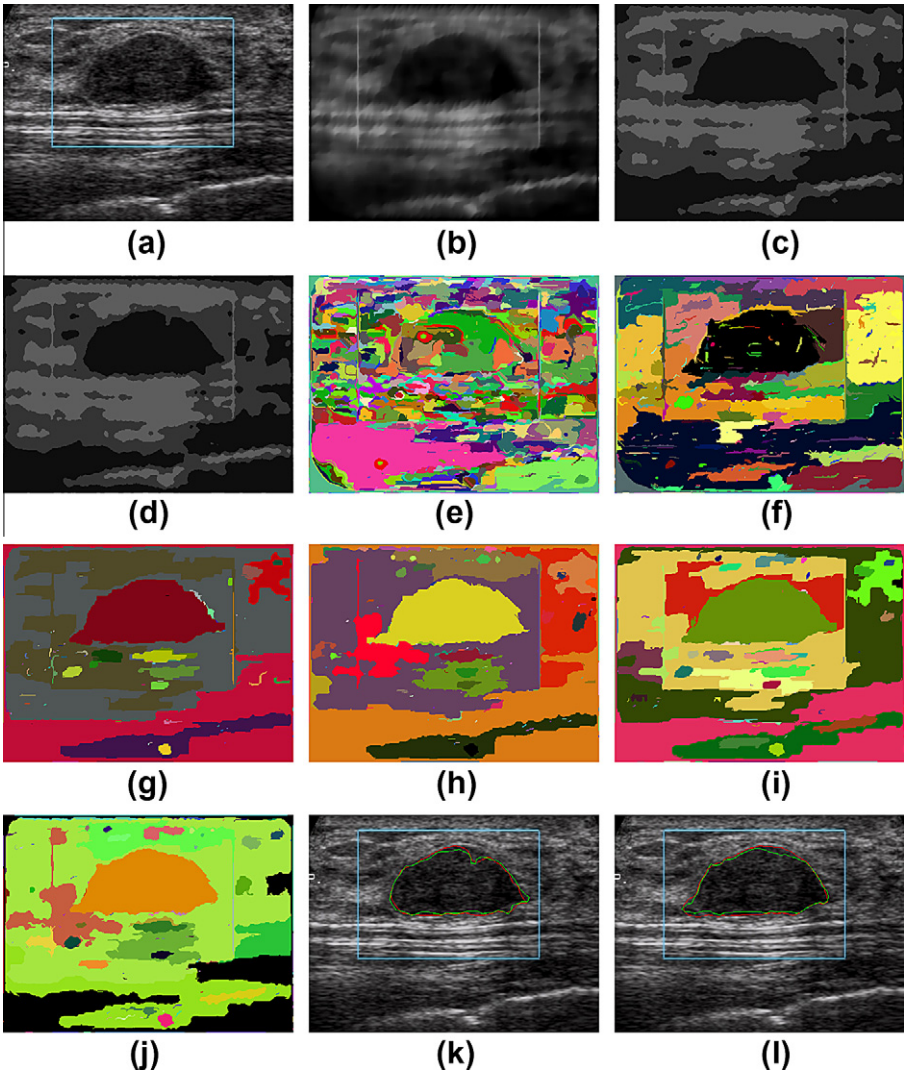

Fig. 5. Segmentation results for the second benign breast tumor. (a) Source image; (b) filtered image; (c) the *K*-means result, $K = 3$; (d) the FCM result, $C = 3$; (e) the EGB result, $k = 150$; (f) the EGB result, $k = 3000$; (g) the RGB result using the 4-connected neighborhood, $k = 2000$, $\alpha = 0.02$; (h) the RGB result using the 6-connected neighborhood (right), $k = 2000$, $\alpha = 0.02$; (i) the RGB result using the 6-connected neighborhood (left), $k = 2000$, $\alpha = 0.02$; (j) the RGB result using the 8-connected neighborhood, $k = 2000$, $\alpha = 0.02$; (k) the FCM + Snake result; and (l) the RGB + Snake result.

As shown in Figs. 4c, 5c, 6c, 7c4d, 5d, 6d, and 7d, the segmentation results of *K*-means and FCM were insensitive to noises when *K* and *c* were relatively small. It can be explained that the smaller cluster number would lead to a so large intensity range for each cluster that the noises with a small variety of intensities would have trivial influence on the clustering results. As shown in Figs. 4e, 5e, 6e and 7e, it is obvious that the EGB method with the $k = 150$ produced the worst segmentation results, where severe over-segmentation can be observed, indicating that the EGB was very sensitive to noises. Even after the *k* could be optimally set so that the breast tumors were better delineated as shown in Figs. 4f, 5f, 6f and 7f, the EGB segmentation results were still sensitive to noises. Worse still, optimized values of *k* were significantly different (1000–5000) for different images to achieve the most acceptable segmented tumors. In some cases, the tumor regions had to be over-segmented so as to be totally separated from the background.

As shown in Figs. 4–7g–j, the segmentation results were robust to noises and much similar for the RGB using the four different types of neighborhood as illustrated in Fig. 1. The parameters were invariable for different images (i.e. *k* was normally set to be 2000, α, 0.01–0.05). Visually, the 4-connected neighborhood has provided sufficient neighboring information to generate the MSTs and obtained neither over- nor under-segmented tumor.

3.2. Quantitative analysis

In experiment 1, an appropriate neighborhood for the RGB could be determined by comparing the computation time and segmentation accuracy of the four types of neighborhood. Theoretically, the time for graph construction and edge mergence is in directly proportional to the number of edges. Given an image with a size of $w \times h$, the number of edges n is

$$n = 2wh - (w + h) \tag{11}$$

for 4-connected neighborhood,

$$n = 3wh - 2(w + h) + 1 \tag{12}$$

for 6-connected neighborhood, and

$$n = 4wh - 3(w + h) + 2 \tag{13}$$

for 8-connected neighborhood.

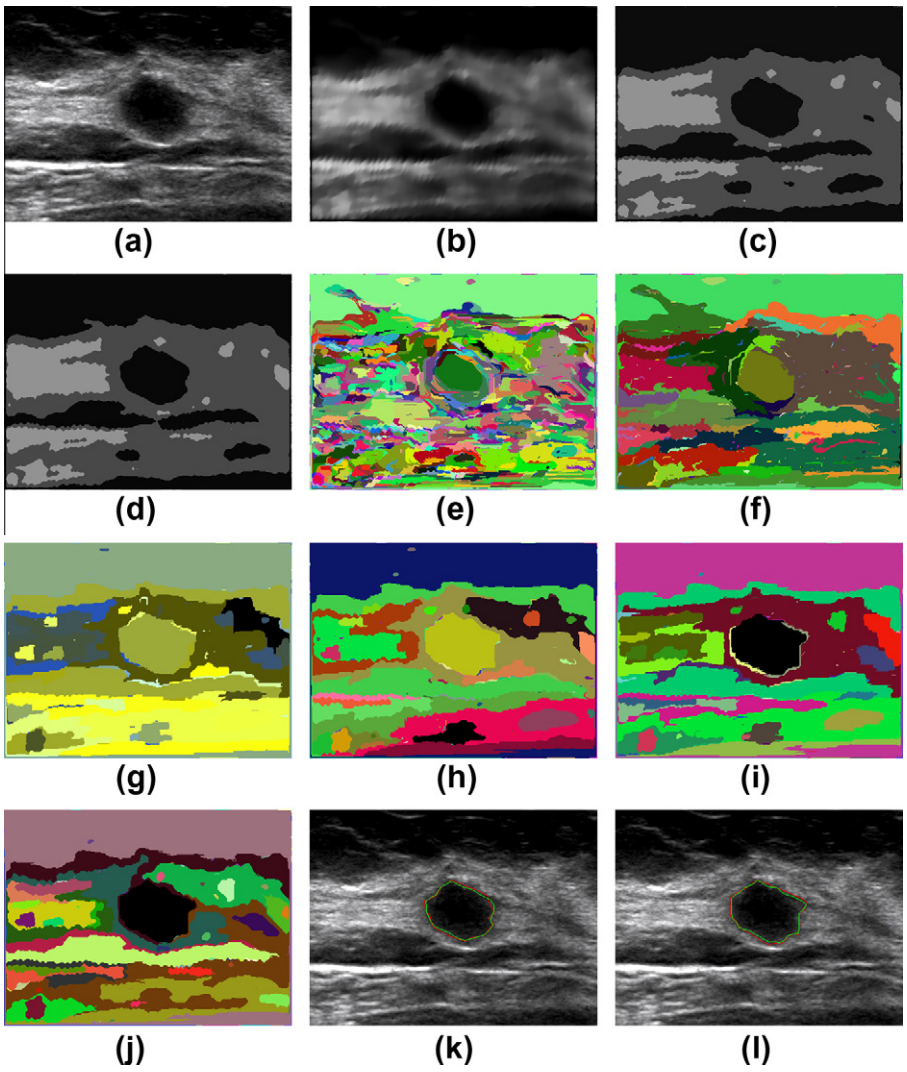

Fig. 6. Segmentation results for the first malignant breast tumor. (a) Source image; (b) filtered image; (c) the *K*-means result, $K = 3$; (d) the FCM result, $C = 3$; (e) the EGB result, $k = 150$; (f) the EGB result, $k = 4000$; (g) the RGB result using the 4-connected neighborhood, $k = 2000$, $\alpha = 0.02$; (h) the RGB result using the 6-connected neighborhood (right), $k = 2000$, $\alpha = 0.02$; (i) the RGB result using the 6-connected neighborhood (left), $k = 2000$, $\alpha = 0.02$; (j) the RGB result using the 8-connected neighborhood, $k = 2000$, $\alpha = 0.02$; (k) the FCM + Snake result; and (l) the RGB + Snake result.

In the procedure of generating MSTs, each edge should be traversed, hence the time complexity is positively proportional to n. Table 2 illustrates the averaged running time of the RGB segmentation for images of benign and malignant tumors with an image size of 400×300 using the four types of neighborhood. The RGB using the 4-connected neighborhood took about 340 ms, that using the 6-connected neighborhoods about 400 ms, and that using the 8-connected neighborhood about 455 ms.

Table 3 shows the segmentation accuracy of the RGB using the four types of neighborhood. For both benign tumors and malignant tumors, the 8-connected neighborhood outperformed the other types of neighborhood in the ARE measures. Interestingly, the 8-connected neighborhood, however, did not outperform the others in the measures of TPVF, FPVF, and FNVF. In general, the 4-connected neighborhood performed the worst result, and the 8-connected neighborhood performed slightly better than the 6-connected neighborhoods. Taking into account the computation time presented in Table 2, the 6-connected neighborhood provided an acceptable balance between the accuracy and the computational efficiency. As a result, we chose to use the 6-connected right neighborhood for the RGB in the following experiments.

In experiment 2, the images were segmented by the *K*-means, FCM, EGB ant RGB methods. Table 4 gives the AREs computed from the segmentation results of the 20 US images. It can be clearly observed that the RGB outperformed the others in that its AREs for both benign and malignant cases were less than 10%, while the AREs of the other three methods were larger than 10%. Moreover, the RGB achieved the lowest standard deviation of ARE which was less than 2.5% for the RGB and more than 2.5% for the other three methods, indicating its good performance in obtaining stable segmentation results. The EGB which was the most sensitive to noises generated the largest ARE results (12.6% for benign cases and 14.0% for malignant cases). In summary, the RGB, which was much more robust to noises in comparison with the EGB, could achieve the most accurate tumor regions for both of benign and malignant breast tumor images. The improvement of segmentation accuracy measured using the ARE was 1.5–5.6% as shown in Table 4.

In experiment 3, the contours extracted from the FCM and RGB results were treated as the initial contours for the Snake in a hybrid segmentation method. Since over-segmentations might occur when using both the RGB and the FCM methods, an initial tumor

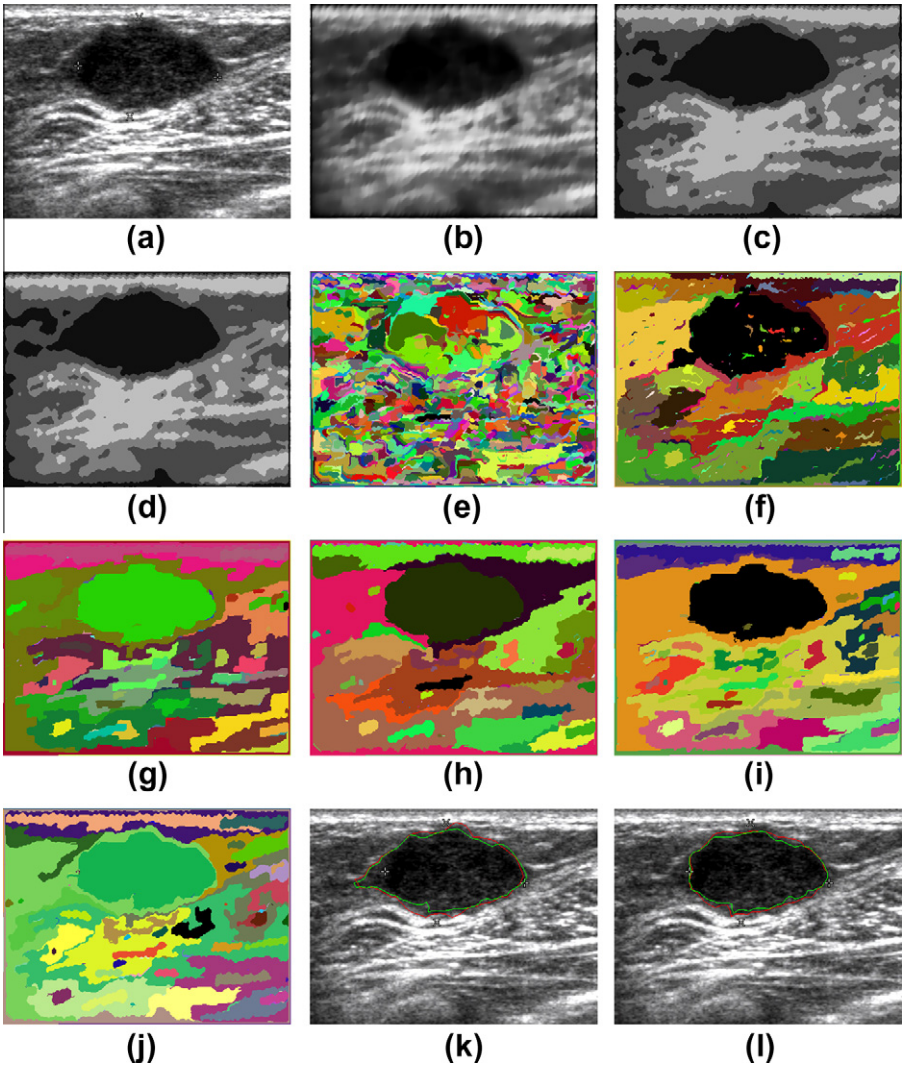

Fig. 7. Segmentation results for the second malignant breast tumor. (a) Source image; (b) filtered image; (c) the *K*-means result, $K = 3$; (d) the FCM result, $C = 3$; (e) the EGB result, $k = 150$; (f) the EGB result, $k = 5000$; (g) the RGB result using the 4-connected neighborhood, $k = 2000$, $\alpha = 0.02$; (h) the RGB result using the 6-connected neighborhood (right), $k = 2000$, $\alpha = 0.02$; (i) the RGB result using the 6-connected neighborhood (left), $k = 2000$, $\alpha = 0.02$; (j) the RGB result using the 8-connected neighborhood, $k = 2000$, $\alpha = 0.02$; (k) the FCM + Snake result; and (l) the RGB + Snake result.

Table 2
The computation time of the RGB using different neighborhoods. The best values are displayed in bold-face type.

Tumor type	Neighborhood	Run time (ms)	Tumor type	Neighborhood	Run time (ms)
Benign	4	**340.6 ± 22.1**	Malignant	4	**340.7 ± 13.6**
	6 Right	396.9 ± 21.2		6 Right	390.7 ± 15.6
	6 Left	404.7 ± 22.5		6 Left	395.3 ± 15.7
	8	456.3 ± 28.5		8	453.4 ± 18.6

contour which might consist of one or more segmented subregions were determined by the three radiologists. Figs. 4k, 5k, 6k and 7k are the segmentation results of FCM + Snake, and Figs. 4l, 5l, 6l and 7l are the segmentation results of RGB + Snake. The initial contours extracted from the FCM or the RGB are in green[1] and the final contours of the Snake are in red.

Tables 5 and 6 show the segmentation performance of the FCM, RGB and hybrid methods applied to the benign and malignant breast tumors, respectively. For the metrics of the ARE, TPVF, and FNVF, it can be clearly seen that the RGB + Snake outperformed the FCM + Snake. For the FPVF, the RGB + Snake had similar performance to the FCM + Snake when applied to the benign tumors, and the latter slightly outperformed the former when applied to the malignant tumors. In addition, the iteration time of the RGB + Snake was on average reduced by a factor of 2.4 comparing with the FCM + Snake. It is worth noting that the Snake could further push the initial contour to the "true" contour as the measures of ARE were approximately improved in both hybrid schemes, indicating that the hybrid scheme should be more practical.

In summary, the RGB provided more accurate segmentations of breast tumors in US images, and furthermore could be used as an

[1] For interpretation of colors in Figs. 4–7, the reader is referred to the web version of this article.

Table 3
The segmentation performance (in percentage) of the RGB using different neighborhoods. The best values are displayed in bold-face type.

Measure	ARE (Mean ± SD)	TPVF (Mean ± SD)	FPVF (Mean ± SD)	FNVF (Mean ± SD)
Benign				
4 Neighborhood	10.5 ± 1.9	84.6 ± 3.9	1.7 ± 1.9	15.4 ± 4.0
6 Neighborhood (right)	9.6 ± 1.4	**87.4 ± 2.5**	**1.6 ± 1.4**	13.8 ± 2.5
6 Neighborhood (left)	9.6 ± 1.7	86.2 ± 3.1	3.5 ± 2.9	**12.6 ± 3.1**
8 Neighborhood	**9.2 ± 1.6**	87.0 ± 3.4	2.5 ± 2.1	13.1 ± 3.4
Malignant				
4 Neighborhood	9.4 ± 3.9	87.1 ± 7.7	4.3 ± 5.5	12.9 ± 7.7
6 Neighborhood (right)	8.5 ± 2.3	**87.6 ± 4.8**	3.3 ± 2.8	**12.3 ± 4.9**
6 Neighborhood (left)	10.0 ± 2.4	87.5 ± 4.5	4.3 ± 5.2	12.4 ± 4.5
8 Neighborhood	**8.1 ± 1.9**	87.3 ± 3.5	**1.8 ± 1.8**	12.7 ± 3.5

Table 4
The ARE (Mean ± SD, in percentage) for the four segmentation methods. The best values are displayed in bold-face type.

Methods	*K*-Means	FCM	EGB	RGB
Benign	11.0 ± 3.4	12.5 ± 3.5	12.6 ± 2.9	**9.5 ± 1.4**
Malignant	14.1 ± 10.0	10.4 ± 3.1	14.0 ± 6.2	**8.5 ± 2.3**

initial contour estimation method for the Snake. The hybrid segmentation scheme combining the RGB and the Snake could more efficiently improve the segmentation performance for the breast US images.

4. Discussions and conclusions

This paper introduces a robust graph-based method (called RGB) for breast tumor segmentation in US images. The RGB which makes use of the regional statistics for determination of whether two connected subregions could be merged is less sensitive to noises in comparison with EGB. Using the NAD model as a preprocessing approach to reducing the speckles, the RGB was successfully applied to 20 breast US images, where benign and malignant tumors were presented. The utilization of regional statistics would theoretically decrease the influence of random noises and was validated by the experimental results. Having carefully selected two parameters k and α, the RGB method illustrated improved robustness to noises and better segmentation performance in comparison with three conventional region based methods, i.e. the *K*-means, the FCM and the EGB. The quantitative experimental results of breast US images have further demonstrated that the proposed RGB method outperformed its counterparts. In addition, we combined the RGB with a classical ACM method, Snake, for achieving more accurate segmentations. The results show that the RGB can be a good initial contour estimation method for the Snake, and the computational efficiency of the Snake can be improved by the hybrid segmentation scheme due to the reduced iterations.

However, the values of k and α were empirically selected in current study, which might be inconvenient for clinicians. According to (6), the parameter k controlled the effect of component size for the minimum internal difference between two subregions,

Table 5
The segmentation performance (in percentage) of the hybrid method for benign breast US images. The best values are displayed in bold-face type.

Parameters of the Snake	Methods	ARE (Mean ± SD)	TPVF (Mean ± SD)	FPVF (Mean ± SD)	FNVF (Mean ± SD)	Iteration time of Snake
1	RGB + Snake	6.5 ± 1.9	91.5 ± 3.7	2.4 ± 3.3	8.5 ± 3.7	14.3 ± 12.4
	FCM + Snake	11.8 ± 5.5	82.5 ± 9.6	1.8 ± 1.7	17.6 ± 9.6	10.5 ± 2.9
2	RGB + Snake	6.6 ± 1.8	90.4 ± 2.4	1.9 ± 1.3	9.6 ± 2.4	11.2 ± 3.4
	FCM + Snake	11.2 ± 4.2	83.0 ± 7.9	2.2 ± 2.4	17.1 ± 7.9	10.7 ± 3.3
3	RGB + Snake	**5.8 ± 1.1**	91.6 ± 2.0	2.2 ± 1.2	8.5 ± 1.9	19.5 ± 9.3
	FCM + Snake	11.1 ± 4.9	83.4 ± 8.9	1.9 ± 1.8	16.7 ± 8.9	27.3 ± 16.8
4	RGB + Snake	8.3 ± 1.8	86.0 ± 3.6	**0.8 ± 0.7**	13.9 ± 3.6	23 ± 16.2
	FCM + Snake	15.4 ± 7.4	75.1 ± 12.9	1.3 ± 1.4	24.9 ± 12.9	23.4 ± 15.1
5	RGB + Snake	5.8 ± 1.2	**91.7 ± 2.1**	2.3 ± 1.7	**8.3 ± 2.1**	**10.3 ± 4.7**
	FCM + Snake	8.8 ± 3.6	87.2 ± 6.4	2.4 ± 2.0	12.8 ± 6.4	15.6 ± 12.2

Table 6
The segmentation performance (in percentage) of the hybrid method for malignant breast tumors. The best values are displayed in bold-face type.

Parameters of the Snake	Methods	ARE (Mean ± SD)	TPVF (Mean ± SD)	FPVF (Mean ± SD)	FNVF (Mean ± SD)	Iteration time of Snake
1	RGB + Snake	6.3 ± 1.8	**91.3 ± 4.4**	**3.3 ± 2.5**	8.6 ± 4.4	18.0 ± 16.3
	FCM + Snake	10.1 ± 6.4	85.1 ± 8.7	8.6 ± 2.8	15.0 ± 8.7	10.5 ± 12.4
2	RGB + Snake	6.0 ± 1.0	88.6 ± 2.1	9.4 ± 1.6	8.7 ± 2.0	9.4 ± 16.8
	FCM + Snake	9.5 ± 6.1	82.7 ± 9.7	9.0 ± 2.9	14.8 ± 9.6	10.6 ± 4.9
3	RGB + Snake	**5.5 ± 1.0**	90.6 ± 1.9	10.0 ± 1.8	7.9 ± 1.9	18.1 ± 15.4
	FCM + Snake	9.9 ± 5.8	79.1 ± 9.1	9.0 ± 3.0	14.1 ± 9.1	22.9 ± 5.4
4	RGB + Snake	7.6 ± 1.8	83.9 ± 3.6	8.3 ± 1.3	11.8 ± 3.6	16.7 ± 16.6
	FCM + Snake	10.8 ± 6.8	72.6 ± 9.2	7.2 ± 2.6	17.8 ± 9.2	18.3 ± 7.6
5	RGB + Snake	5.7 ± 1.1	87.4 ± 2.1	9.8 ± 1.6	**7.5 ± 2.1**	**8.1 ± 19.3**
	FCM + Snake	9.2 ± 7.0	79.4 ± 8.6	9.5 ± 2.9	12.2 ± 8.5	22.3 ± 18.3

$MInt(C_1, C_2)$. Larger k tended to make the region mergence easier as the threshold function $\tau(C)$ as well as $MInt(C_1, C_2)$ was increased, weakening the evidence of the boundary between C_1 and C_2, and vice versa. Therefore, a careful assignment of k should be important to obtain a user-defined balance between the over- and under-segmentations. Similarly, the parameter α adjusted the influence of component size on the threshold function based on the SNR measures. In current study, α could only be empirically set. We have found $k = 2000$ and $\alpha = 0.01–0.05$ for benign and malignant tumors and illustrated their usefulness for our US data sets in the experiments. Through experiments, it is noted that the selections of k and α seems to be different for different image sizes and object sizes. For US images containing breast tumors, it would be possible to find optimal or suboptimal k and α that can achieve satisfactory segmentation results by using a larger amount of data.

In our future work, we will study the relationship between the optimal parameter values and the size of the image, and apply some intelligent machine learning methods (e.g. evolutionary computation) for automatically obtaining the optimal parameter values based on a larger amount of breast tumor images. Moreover, fully automatic segmentation scheme based on the RGB method will be investigated to automatically locate the target segments, even when over-segmentation is presented. It is expected that the RGB based segmentation method and the hybrid scheme presented in this paper can be used for a variety of clinical applications.

Acknowledgments

We would like to thank Professor Chien Ting Chin from Shenzhen University, China, and the anonymous referees for their great help in improving the quality of the paper. This work was supported by the Program for New Century Excellent Talents in University, Ministry of Education, China (No. NCET-10-0363), the Basic Science Research Fund of Shenzhen (No. JC20100602 0025A), the Fundamental Research Funds for the Central Universities, SCUT (Nos. 2009ZM0059, 2009ZZ0014) and National Natural Science Funds of China (Nos. 61001181, 60901015 and 61075021).

References

[1] G.F. Xiao, M. Brady, J.A. Noble, Y.Y. Zhang, Segmentation of ultrasound B-mode images with intensity inhomogeneity correction, IEEE Trans. Med. Imag. 21 (1) (2002) 48–57.
[2] A. Sanfeliu, R. Alquezar, J. Andrade, J. Climent, F. Serratosa, J. Verges, Graph-based representations and techniques for image processing and image analysis, Pattern Recogn. 35 (3) (2002) 639–650.
[3] X.J. Zhu, P.F. Zhang, J.H. Shao, Y.Z. Cheng, Y. Zhang, J. Bai, A snake-based method for segmentation of intravascular ultrasound images and its in vivo validation, Ultrasonics 51 (2) (2011) 181–189.
[4] J.A. Noble, D. Boukerroui, Ultrasound image segmentation: a survey, IEEE Trans. Med. Imag. 25 (8) (2006) 987–1010.
[5] M. Kass, A. Witkin, D. Terzopoulos, Snakes – active contour models, Int. J. Comput. Vision 1 (4) (1987) 321–331.
[6] Y.L. Huang, D.R. Chen, Automatic contouring for breast tumors in 2-D sonography, in: Proceedings of the 2005 IEEE Engineering in Medicine and Biology, Shanghai, China, 2005, pp. 3225–3228.
[7] R.F. Chang, W.J. Wu, C.C. Tseng, D.R. Chen, W.K. Moon, 3-D snake for US in margin evaluation for malignant breast tumor excision using mammotome, IEEE Trans. Inf. Technol. Biomed. 7 (3) (2003) 197–201.
[8] A.K. Jumaat, W.E.Z.W.A. Rahman, A. Ibrahim, R. Mahmud, Comparison of Balloon Snake and GVF Snake in Segmenting Masses from Breast Ultrasound Images, ICCRD, Kuala Lumpur, Malaysia, 2010, pp. 505-509.
[9] G. Hamameh, T. Gustavsson, Combining snakes and active shape models for segmenting the human left ventricle in echocardiographic images, in: Proceedings of Computers in Cardiology, Cambridge, MA, USA, 2000, pp. 115–118.
[10] K.Y.E. Leung, M.V. Stralen, G.V. Burken, N.D. Jong, J.G. Bosch, Automatic active appearance model segmentation of 3D echocardiograms, in: Proceedings of ISBI, Rotterdam, Netherlands, 2010, pp. 320–323.
[11] G. Liu, B. Wang, D.C. Liu, Detection of intima-media layer of common carotid artery with dynamic programming based active contour model, in: Proceedings of CCPR, Beijing, China, 2008, pp. 369–374.
[12] S.G. Moursi, M.R. El-Sakka, Initial contour for ultrasound carotid artery snakes, in: Proceedings of ISSPIT, Cairo, Egypt, 2007, pp. 390–395.
[13] Y. Zhang, W. Qian, R. Sankar, Prostate boundary detection in transrectal ultrasound images, in: Proceedings of ICASSP, Philadelphia, PA, USA, 2005, pp. V617–V620.
[14] R. Medina, A. Bravo, P. Windyga, J. Toro, P. Yan, G. Onik, A 2-D active appearance model for prostate segmentation in ultrasound images, in: Proceedings of the 2005 IEEE Engineering in Medicine and Biology, Shanghai, China, 2005, pp. 3363–3366.
[15] D.E. Maroulis, M.A. Savelonas, D.K. Iakovidis, S.A. Karkanis, N. Dimitropoulos, Variable background active contour model for computer-aided delineation of nodules in thyroid ultrasound images, IEEE Trans. Inf. Technol. Biomed. 11 (5) (2007) 537–543.
[16] A. Zaim, J. Jankun, An energy-based segmentation of prostate from ultrasound images using dot-pattern select cells, in Proceedings of ICASSP, Honolulu, HI, USA, 2007, pp. I297–I300.
[17] R.O. Duda, P.E. Hart, D.G. Stork, Pattern Classification, second ed., Wiley-Interscience, USA, 2000.
[18] D. Boukerroui, O. Basset, A. Baskurt, A. Hernandez, N. Guerin, G. Gimenez, Texture based adaptive clustering algorithm for 3D breast lesion segmentation, in: Proceedings of IEEE Ultrasonics Symposium, Toronto, Canada, 1997, pp. 1389–1392.
[19] S. Poonguzhali, B. Deepalakshmi, G. Ravindran, Optimal feature selection and automatic classification of abnormal masses in ultrasound liver images, in: Proceedings of ICSPCN, Chennai, India, 2005, pp. 503–506.
[20] K.B. Jayanthi, R.S.D.W. Banu, Carotid artery boundary extraction using segmentation techniques: a comparative study, in: Proceedings of ITNG, Las Vegas, NV, USA, 2009, pp. 1290–1295.
[21] P.F. Felzenszwalb, D.P. Huttenlocher, Image segmentation using local variation, in: Proceedings of IEEE Computer Society Conference on Computer Vision and Pattern Recognition, Santa Barbara, CA, USA, 1998, pp. 98–104.
[22] F. Ma, M. Bajger, J.P. Slavotinek, M.J. Bottema, Two graph theory based methods for identifying the pectoral muscle in mammograms, Pattern Recogn. 40 (9) (2007) 2592–2602.
[23] P.F. Felzenszwalb, D.P. Huttenlocher, Efficient graph-based image segmentation, Int. J. Comput. Vision 59 (2) (2004) 167–181.
[24] Y.Y. Shu, G.A. Bilodeau, F. Cheriet, Segmentation of laparoscopic images: integrating graph-based segmentation and multistage region merging, in: Proceedings of 2nd Canadian Conference on Computer and Robot Vision, Victoria, BC Canada, 2005, pp. 429–436.
[25] H. Susukida, F. Ma, M. Bajger, Automatic tuning of a graph-based image segmentation method for digital mammography applications, in: Proceedings of ISBI, Paris, France, 2008, pp. 89–92.
[26] K.Z.A. Elmoniem, A.B.M. Youssef, Y.M. Kadah, Real-time speckle reduction and coherence enhancement in ultrasound imaging via nonlinear anisotropic diffusion, IEEE Trans. Biomed. Eng. 49 (9) (2002) 997–1014.
[27] Y. Chen, R.M. Yin, P. Flynn, S. Broschat, Aggressive region growing for speckle reduction in ultrasound images, Pattern Recogn. Lett. 24 (4–5) (2003) 677–691.
[28] C.T. Zahn, Graph–theoretical methods for detecting and describing gestalt clusters, IEEE Trans. Comput. c-20 (1) (1971) 68–86.
[29] J.B. Kruskal, On the shortest spanning subtree of a graph and the traveling salesman problem, Proc. Am. Math. Soc. 7 (1) (1956) 48–50.
[30] J.W. Donna, S. Mubarak, A fast algorithm for active contours and curvature estimation, CVGIP: Image Understand 55 (1) (1992) 14–26.
[31] J.K. Udupa, V.R. LaBlanc, H. Schmidt, C. Imielinska, P.K. Saha, G.J. Grevera, Y. Zhuge, P. Molholt, Y.P. Jin, L.M. Currie, A methodology for evaluating image segmentation algorithms, in: Proceedings of Medical Imaging, San Diego CA, 2002, pp. 266–277.